

Supplemental Methods, Figures and Tables

Proteomic, biomechanical, and functional analyses define neutrophil heterogeneity in systemic lupus erythematosus.

Kathleen R. Bashant, Angel M. Aponte, Davide Randazzo, Paniz Rezvan Sangsari, Alex JT Wood, Jack A. Bibby, Erin E. West, Arlette Vassallo, Zerai Manna, Martin P. Playford, Natasha Jordan, Sarfaraz Hasni, Marjan Gucek, Claudia Kemper, Andrew Conway Morris, Nicole Y. Morgan, Nicole Toepfner, Jochen Guck, Nehal N. Mehta, Edwin R. Chilvers, Charlotte Summers, Mariana J. Kaplan

Supplemental Methods

Human subjects: All studies were approved by site-specific IRBs, including the Cambridge Local Research Ethics Committee (REC reference 06/Q0108/281) and NIAMS IRB (NIH 94-AR-0066). All subjects signed informed consent. Subjects with SLE fulfilled the American College of Rheumatology revised criteria for SLE¹. Subjects were recruited from the University of Cambridge and the NIAMS Lupus Clinics (Supplementary Table 2). Healthy volunteers were recruited by advertisement.

Peripheral blood venipuncture: Blood was drawn by venipuncture and collected into 3.8% sodium citrate tubes (Sarstedt, Numbrecht, Germany)

Neutrophil isolation: Percoll (Sigma-Aldrich, Dorset, UK)³ or Ficoll (Sigma-Aldrich, MO, USA)⁴ discontinuous gradients were used, as described previously, to separate erythrocytes and granulocytes from peripheral blood mononuclear cells. Normal dense neutrophils were separated from erythrocytes using the EasySep direct neutrophil isolation kit (StemCell Technologies, MA, USA). Low dense neutrophils were purified from the PBMCs using the same EasySep neutrophil isolation kit with customized antibodies targeting CD86 and HLA-DR4 (StemCell Technologies, MA, USA). Cells were counted using a hemocytometer. Cytospin slides were prepared for each neutrophil preparation and cell purity was assessed by light microscopy. Cells prepared in this manner were routinely >95% neutrophils. For specific experiments, cells were resuspended at 5

million/mL in phosphate buffer saline (PBS) (Sigma-Aldrich, MO, USA) (Sigma-Aldrich, Dorset, UK) and rested for 20 minutes at 37°C. Neutrophils were subsequently exposed to fMLF (Sigma-Aldrich, MO, USA) (Sigma-Aldrich, Dorset, UK), IFN α (Sigma-Aldrich, Dorset, UK), SmRNP immune complexes (Arotech Diagnostics, Wellington, NZ) ⁵, 0.1 μ M cytochalasin D (Thermo Fisher Scientific, MA, USA), dimethyl sulfoxide (DMSO), or autologous/heterologous serum at the dosages and times described in the text.

Generation of immune complexes: SLE-specific immune complexes were generated as previously described [49]. In brief, serum samples from SLE patients within the NIH lupus cohort expressing high titers of anti-RNP/Sm antibodies were identified. Age/sex/race-matched control sera was also identified. IgG was purified from these samples via the Melon Gel IgG spin purification kit (Thermo Fisher Scientific). Gel electrophoresis was performed to assess IgG purity. Colloidal blue stain indicated protein bands at 150 kDa, the molecular weight for IgG, as well as at 25kDa and 50kDa (heavy and the light chains respectively). These results matched those in the Melon purification manual. To generate immune complexes, purified IgG or commercially available BSA IgG (AbCam ab19260) were incubated with U1 RNP/Sm antigen (Arotech Diagnostics ATR01-10) or BSA (2mg/ml, Thermo Fisher Scientific) respectively at a 1:1 ratio for 30 minutes at room temperature. Neutrophils were exposed to 10 μ g/ml of immune complexes or IgG for induction of NETs.

Induction of NETs: Neutrophils purified by ficoll gradient were resuspended in RPMI-1640 (Life Technologies). Poly-L-lysine (Sigma-Aldrich) pre-coated coverslips were placed in each well of a 24 well plate. 1*10⁶ neutrophils/ml were exposed to 10 μ g/ml of IgG or immune complexes, 500ng/ml PMA (Sigma-Aldrich), or no additional stimulus for 4 hours at 37°C. Total sample volume was 50 μ l. After 4 hours, 1mL of 4% paraformaldehyde was placed over the sample and the plate was incubated at 4°C overnight.

Visualization of platelets and NETs: Coverslips of neutrophils were imaged as previously described [50]. In brief, coverslips were washed, then incubated at room temperature with 0.2% gelatin for 30 minutes. After washing, coverslips were incubated 1 hour at 37°C with anti-myeloperoxidase (MPO; 1:1000, Jackson ImmunoResearch) or anti-CD41a (1:1000, ThermoFisherScientific) as indicated in the figure legends. After washing, coverslips were incubated 30 minutes at 37°C with secondary fluorochrome-conjugated antibodies (1:400, Jackson ImmunoResearch). After washing, coverslips were stained with Phalloidin (ThermoFisherScientific) and/or Hoechst (1:1000, Thermo Fisher Scientific) as indicated in the figure legends. Coverslips were mounted with ProLong Gold Antifade (Thermo Fisher Scientific) and three images/slide were taken with a Leica 4000B inverted light microscope (Leica Microsystems) with a x40 objective.

Quantification of NETs: Netting neutrophils were manually counted (MPO and DAPI-colocalization on strand-like DNA structures) and divided by the total number of cells (DAPI-only and MPO/DAPI-colocalization) under blinded conditions. An average value for percentage of neutrophils undergoing NET formation on each slide was calculated.

Preparation of lysates for proteomics: NDNs and LDGs were isolated from SLE patients and age/sex-matched healthy volunteers. Cells were resuspended at 10 million/mL in PBS and rested for 25 minutes at 37°C with or without 100nM fMLF. Samples were centrifuged at 400g for 5 minutes at 4°C, supernatants were aspirated, and cell pellets were snap frozen in liquid nitrogen. Ice cold lysis buffer with 0.5% sodium dodecyl sulfate (SDS) (Sigma-Aldrich, MO, USA), 0.1M tetraethylammonium bromide (TEAB) (Thermo Fisher Scientific, MA, USA), and 1X HALT™ protease and phospho-protease inhibitor cocktail (Thermo Fisher Scientific, MA, USA) (200µL) was added to each cell pellet and cells were mechanically lysed for 10 minutes. Lysates were

centrifuged at 20,000g for 10 minutes at 4°C, the supernatant was removed, and the protein was stored at -70°C. Protein integrity was assessed by SDS-polyacrylamide gel electrophoresis (PAGE) and colloidal blue staining (Thermo Fisher Scientific, MA, USA). Lysate protein concentrations were determined by bicinchoninic acid (BCA) assay (Bio-Rad, CA, USA).

11-Plex TMT labeling: Approximately, 40µg of protein per sample and internal standard (pooled equivalent amounts of each sample) were reduced in 5 mM Tris(2-carboxyethyl)phosphine (TCEP) for one hour at 55°C, which was followed by alkylation of cysteines with 18mM iodoacetamide for 30 minutes in the dark at room temperature. Six volumes of chilled acetone were added, and precipitation proceeded overnight. Lysates were resuspended in 0.1M TEAB before trypsin was added at a 1:40 trypsin:protein ratio by mass. Digestion was carried out overnight at 37°C. Tandem mass tag (TMT) reagents (0.4 mg) were reconstituted in 41µL anhydrous acetonitrile and peptide samples were labelled according to the manufacturer's protocol. Following incubation at room temperature for one hour, the reaction was quenched with hydroxylamine to a final concentration of 5% (v/v) for 15 min at room temperature. The TMT-labelled samples including internal standard were pooled across the 11 samples for each TMT set (patient, healthy volunteer). Pooled TMT sample sets were concentrated and desalted using Oasis HLB 1 cc cartridge (Waters). The pooled samples were vacuum centrifuged to dryness and subjected to basic pH reversed-phase (bRP) fractionation.

Offline Reversed-Phase Fractionation: For each TMT set, high pH reversed-phase liquid chromatography was performed on an offline Agilent 1200 series HPLC. Approximately, 0.44 mgs of desalted peptides from each set were resuspended in 0.1 ml 10 mM triethyl ammonium bicarbonate with 2% (v/v) acetonitrile. Peptides were loaded onto an Xbridge C₁₈ HPLC column (Waters; 2.1mm inner diameter x 100 mm, 5µm particle size), and profiled with a linear gradient of 5–35 % buffer B (90% acetonitrile, 10 mM triethyl ammonium bicarbonate) over 60 min, at a

flowrate of 0.25 ml/min. The chromatographic performance was monitored by sampling the eluate with a diode array detector (1200 series HPLC, Agilent) scanning between wavelengths of 200 and 400 nm. Fractions were collected at 1 min intervals followed by fraction concatenation⁶. 15% (v/v) of each of the 12 concatenated fractions were separated into a new tube dried and resuspended in 0.01% formic acid, 2% acetonitrile for full proteome analysis. Approximately 500 ng of peptide fraction mixture was loaded per liquid chromatography-mass spectrometry run. The remaining volume in each fraction was subjected to phosphopeptide enrichment.

Phosphoprotein enrichment: The initial 12 fractions were combined into 6 fractions and sequential metal oxide affinity chromatography (SMOAC) phosphopeptide enrichment was performed. Briefly, TMT labeled tryptic digest was subjected to the High-Select TiO₂ Phosphopeptide Enrichment kit according to manufacturer's protocol (Thermo Fisher Scientific). The TiO₂ eluent was saved for MS analysis. The TiO₂ flow through and wash fractions were pooled, and the phosphopeptides were enriched using the High-Select Fe-NTA Phosphopeptide Enrichment kit according to manufacturer's protocol (Thermo Fisher Scientific), eluent was saved for MS analysis.

Mass Spectrometry: All fractions were analyzed on an Ultimate 3000-nLC coupled to an Orbitrap Fusion Lumos Tribrid instrument (Thermo Fisher Scientific) equipped with a nanoelectrospray source. Peptides were separated on an EASY-Spray C₁₈ column (75 µm x 50cm inner diameter, 2 µm particle size and 100 Å pore size, Thermo Fisher Scientific). Peptide fractions were placed in an autosampler and separation was achieved by 120 min gradient from 4-32% buffer B (100% ACN and 0.1% formic acid) at a flow rate of 300 nL/min. An electrospray voltage of 1.9 kV was applied to the eluent via the EASY-Spray column electrode. The Lumos was operated in positive ion data-dependent mode, using Synchronous Precursor Selection (SPS-MS3)⁷. Full scan MS1 was performed in the Orbitrap with a precursor selection range of 375–1,275 m/z at nominal

resolution of 1.2×10^5 . The AGC target and maximum accumulation time settings were set to 4×10^5 and 50 ms, respectively. The top ten precursors were then selected for MS2/MS3 analysis. MS2 was triggered by selecting the most intense precursor ions above an intensity threshold of 5×10^4 for collision induced dissociation (CID)-MS2 fragmentation with an AGC target and maximum accumulation time settings of 1×10^4 and 90 ms, respectively. Mass filtering was performed by the quadrupole with 0.7 m/z transmission window, followed by CID fragmentation in the linear ion trap with 35% normalized collision energy in rapid scan mode and parallelizable time option was selected. SPS was applied to co-select 10 fragment ions for HCD-MS3 analysis. SPS ions were all selected within the 400–1,200 m/z range and were set to preclude selection of the precursor ion and TMTc ion series⁸. The AGC target and maximum accumulation time were set to 1×10^5 and 150 ms (respectively) and parallelizable time option was selected. Co-selected precursors for SPS-MS3 underwent HCD fragmentation with 65% normalized collision energy and were analyzed in the Orbitrap with nominal resolution of 5×10^4 .

Proteomics Analysis: Raw data files were processed using Proteome Discoverer (v2.4, Thermo Fisher Scientific), with Sequest HT (Thermo Fisher Scientific) search node. All peak lists were searched against the UniProtKB/Swiss-Prot protein database released 2019_11 with Homo sapiens taxonomy (20,316 sequences) and concatenated with reversed copies of all sequences. The following search parameters were set with fixed modifications carbamidomethylation of Cys, TMT 11-plex modification of lysines and peptide N-terminus; variable modification of methionine oxidation. For SPS-MS3 the precursor and fragment ion tolerances were set to 10 ppm and 0.6 Da, respectively. Up to two-missed tryptic cleavages were permitted. Percolator algorithm (v.3.02.1, University of Washington) was used to calculate the false discovery rate (FDR) of peptide spectrum matches (PSM), set to a q-value <0.05 ⁹⁻¹².

Proteins were quantified by summing reporter ion counts across all matching PSMs, also as

described previously¹³. Reporter ion intensities were adjusted to correct for the isotopic impurities of the different TMT reagents according to manufacturer specifications. The signal-to-noise (S/N) measurements of peptides assigned to each protein were summed and these values were normalized so that the sum of the signal for all proteins in each channel was equivalent to account for equal protein loading. Finally, each protein abundance measurement was scaled to internal standard channels to reduce multibatch variability¹⁴. The p-values were calculated for the reported quantitative ratios using ANOVA testing.

Data from the phosphopeptide enrichment were processed and quantified similarly except an additional variable modification of phosphate on serine, threonine, and tyrosine residues was included as a Sequest search parameter. Quantitative values were based at the peptide group level for site specific phosphorylation quantitation. For more detail into the proteomics method used, see¹⁵.

Network Mapping: Network mapping to GO biological processes was performed using opensource software ShinyGo¹⁶ and online platform MetaScape¹⁷. Proteins upregulated with an abundance ratio of >1.5 or downregulated with an abundance ratio of <0.5 in at least four of the five matched samples were included in network mappings to account for individual variation. For phospho-proteomics, proteins with differential phosphorylation at a given phospho-site in at least 4/5 matched samples were included. False discovery rate (FDR) was used to rank enriched networks based on significance. Heatmaps were generated in GraphPad Prism to display relative protein expression in different neutrophil subsets.

Real-time Deformability Cytometry: RT-DC was performed as described previously^{18 19}. In brief, neutrophils were resuspended by gentle mixing in CellCarrier buffer (Zellmechanik Dresden GmbH, Germany) at concentrations of 2.5×10^7 cells/mL. CellCarrier is based on $1 \times$ PBS buffer

containing 0.5% methylcellulose. Cell suspensions were drawn into 1 mL syringes and placed in a syringe pump (neMESYS, Cetoni GmbH, Korbussen, Germany) of the AcCellerator (Zellmechanik Dresden GmbH, Germany), an extension for an inverted microscope. Syringes were connected to polymer tubing, which was attached to the sample inlet of a Flic20 PDMS microfluidic chip (Zellmechanik Dresden GmbH, Germany). The chip contains reservoirs that are connected by a square measurement channel with a $20 \times 20 \mu\text{m}^2$ cross-section. Another syringe without cells was filled with CellCarrier buffer, placed in the syringe pump, and connected to the sheath inlet of the microfluidic chip. RT-DC measurements were collected at a cellular flow rate of $0.12 \mu\text{L/s}$ ($0.03 \mu\text{L/s}$ sample flow and $0.09 \mu\text{L/s}$ sheath flow). For isolated cell populations, an open gating strategy was employed. For whole blood measurements, $50 \mu\text{L}$ blood was diluted into $950 \mu\text{L}$ CellCarrier buffer and a gate for cells sized $5\text{--}16 \mu\text{m}$ parallel to and $5\text{--}20 \mu\text{m}$ perpendicular to flow direction was applied. This was sufficient to exclude single erythrocytes and erythrocyte doublets. An inverted microscope in combination with a high-speed CMOS camera (Mikrotron GmbH, Unterschleißheim, Germany) captured images of cells at a frame rate of 2000 frames per second as they reached the end of the constriction channel. Real-time image analysis was performed during the measurement process and data files necessary for single-cell MORE analysis (see below) exported for all detected cells.

Morpho-Rheological Analysis: Previous reports have already described methods to analyze RT-DC data files²⁰⁻²². In brief, a cell tracing algorithm implemented in C/LabVIEW, in combination with off-line analysis using ShapeOut software and custom-written Python scripts allow for generation of a neutrophil morpho-rheological or “MORE” profile. For each cell detected, data describing a bright field image of the cell, the contour of the cell, and the cell size (as the cross-sectional area of the cell) were exported and analyzed. Cell size was obtained from the area inside the convex hull, a processed contour, where all points contributing to concave curvature

were removed. Deformation is a measure of the cell's deviation from sphericity and is calculated from the convex hull of the cell:

$$\text{Deformation} = 1 - \frac{2\sqrt{\pi A}}{l},$$

where A is the convex hull area and l is the length of the convex hull perimeter. Pre-existing shape deviations from sphericity were controlled for by analyzing cells within a reservoir devoid of stresses in front of the constriction channel. In this manner, cellular deformation due to constriction stresses alone was obtained and presented. The ratio of convex hull area to cell contour area is defined as the cellular area ratio and provides a measure of cell surface roughness. Cells with area ratios in the range of 1.0–1.05 were used to compare leukocyte deformation and size. The mean brightness of the cell was determined using all pixel values falling within the cell's contour. Major leukocyte subpopulations were identified based on cell size and mean brightness. Red blood cells were identified due to their extremely deformable state within the constriction channel. For further detailed information, see ²².

Ibidi endothelial flow assay: Human pulmonary microvascular endothelial cells (HMVEC-P) (AngioProteomie, MA, USA) were grown to 80% confluence on 75 cm² flasks in endothelial cell growth MV2 medium with 2% fetal calf serum (FCS) (AngioProteomie, MA, USA). The cells were lifted off the flasks using 6 mL of TrypLE Express (Thermo Fisher Scientific, MA, USA) for 3 minutes, neutralized with 12 mL of MV2 medium. The cells were centrifuged at 260g for 3 minutes, and the supernatant removed, before being re-suspended in medium at 1 million/mL. 120 μL of cell suspension was transferred to Ibidi® μ-slide VI 0.4 chambers (Ibidi, WI, USA) and grown to confluence overnight at 37°C in 5% CO₂. Human neutrophils were isolated as defined above and suspended in PBS at a concentration of 1 million/mL. Where indicated, endothelial cells were treated with 0.4 ng/mL of IFNγ (Thermo Fisher Scientific, MA, USA) and TNFα (Thermo Fisher Scientific, MA, USA) for 4 hours. The confluent endothelial cells were washed for 2 minutes with

PBS at 0.4mL/minute. Cells were imaged using a DMI6000 inverted microscope (Leica) using an oil immersion Plan-Apo 20X/0.8 numerical aperture (NA) objective (Leica). During the entire experiment, cells were constantly maintained at controlled temperature (37°C) and CO₂ (5%). Neutrophils were flowed across the endothelial surface for 3 minutes at the same rate. Time-lapse recordings were captured using a cooled Andor EM-CCD camera driven by the LAS X software (Leica) at a rate of 56fps to evaluate neutrophil-endothelial interactions. The percentage of neutrophils adhering to or rolling alongside the endothelium out of the total number of neutrophils flowing past the field of view was calculated for SLE LDGs, SLE NDNs, HC NDNs, and primed HC NDNs. Rates of interaction with the endothelium for different neutrophil subsets were compared.

PDMS microvasculature mimetic: To mimic the trafficking of cells in pulmonary vasculature, we developed the microvasculature mimetic (MM). After conceptualization, the design was undertaken using L-Edit (Mentor Graphics) for the MM: a branched pyramidal network without constrictions (constant width of 15 µm). A polyester photomask of the designs was printed commercially (Fineline Imaging, CO, USA). Using the photomask, the master molds were fabricated at the Biomedical Engineering and Physical Science Shared Resource in the National Institute of Biomedical Imaging and Bioengineering following standard photolithographic techniques. Briefly, SU-8 2015 (Kayaku Advanced Materials, Westborough MA) was deposited on silicon wafer substrates using a spin-coater (Laurell Technologies, PA, USA), prebaked, patterned using the masks and a collimated light source (OAI Instruments, CA, USA), post-exposure baked, and developed. To increase durability, the master molds were hard-baked at 150°C for 2 minutes, after which they were treated with a vapor of (tridecafluoro-1,1,2,2-tetrahydrooctyl)-1-trichlorosilane (UCT Specialties, PA, USA) in a vacuum desiccator for one hour. For soft lithography, PDMS (Sylgard 184, Dow Corning) was combined in a 10:1 w:w ratio of base to curing agent in a planetary mixer (THINKY, CA, USA), then poured onto the master

molds, briefly degassed under vacuum, and baked for 45 minutes at 80°C. After demolding the cured PDMS and cutting out the device, inlet and outlet holes were punched (Acuderm, 1.5mm punch). The PDMS devices were cleaned with tape in a HEPA filtered hood and bonded to glass cover slips using oxygen plasma (PE-100, Plasma Etch, USA). Using one device at a time for experiments, the inlet and outlet were connected to a microfluidic pressure control unit (Flow-EZ, Fluigent) using polyethylene tubing (Scientific Commodities, AZ, USA), such that less than 500 μL of cell suspension was introduced for each experiment. Cells were suspended in PBS at 3.33×10^5 cells/mL and flowed through the microchannels using driving pressures within the physiological range (25, 50, and 100 mbar). For imaging, the device was mounted on a DMI6000 inverted widefield microscope (Leica). Imaging was performed using a Plan-Apo 10X/0.45NA objective (Leica) to measure the transit time through the entire device. During the entire experiment, cells were constantly maintained at controlled temperature (37°C) and CO₂ (5%). Time-lapse recordings were captured using a cooled Andor EM-CCD camera driven by the LAS X software (Leica) at a rate of 56fps. Transit times were extracted from the videos manually. The concept of using a PDMS mimetic for the pulmonary microvasculature to study neutrophil trafficking was inspired by²³ but in this work we opted for a branched channel network rather than a single channel with constrictions. Viability testing was completed using trypan blue (Thermo Fisher Scientific, MA, USA). Transit times were calculated manually and represent the difference between the times of a given cell entering and exiting the mimetic.

Brightfield and lattice light-sheet fluorescence microscopy: Neutrophils were suspended in Hank's Buffered Salt Solution with 25 mM N-(2-Hydroxyethyl)piperazine-N'-(2-ethanesulfonic acid) (HEPES) (Thermo Fisher Scientific, MA, USA), at a concentration of 1 million/mL. 200 μL of cell solutions was aliquot into an 8-well glass chamber slide (Ibidi, WI, USA). Cells were concomitantly stained with 167nM sytox green (Thermo Fisher Scientific, MA, USA) and 500nM of SiR-Actin (Spirochrome, CO, USA) for 30 minutes, kept at 37°C and 5% CO₂. Brightfield and

fluorescence live recordings of actin changes in response to priming with 100 nM fMLF or 25 nM PMA (Sigma-Aldrich, MO, USA) were acquired using a Zeiss Lattice Lightsheet 7 inverted microscope equipped with a Plan-Apo 48X/1.0NA detection objective, a cooled PCO.edge sCMOS camera and driven by the Zen Blue 3.1 software (Zeiss). Brightfield images were obtained by illumination of samples with white LED light. As for fluorescence acquisition, a 650nm-waist light sheet was employed. Image volumes were acquired with a lateral translation of 0.2 μ m, and the 488nm and 640nm laser lines were used for Sytox green and SiR-Agin (shown in red), respectively. Time-lapse recordings were acquired in dithering mode and then deconvolved in the processing module of the Zen Blue 3.1 software applying the “Constrain Iterative” algorithm. Data were then transformed (“deskewed”) to achieve a conventional x, y, z visualization and exported as .CZI files. Finally, data were imported into IMARIS 9.5.1 software (Bitplane) for processing. Neutrophils were visually inspected to compare morphologies.

Analysis of RNA sequencing: For analysis of the RNA-sequencing data, raw counts for SLE patients were obtained from GSE139358 and counts for HC NDNs cultured with or without heat-killed *Staphylococcus Aureus* were obtained from GSE73313. Data were then TMM normalized using the EdgeR package (REF). No filtering of genes based on expression level was done as undetected genes were informative in the analysis. All subsequent data were then plotted using counts per million (CPM) values. For comparisons to RNA-sequencing data, proteomic abundances were converted to abundance per million data (referred to here as CPM). Generation of complement datasets was done through combining unique genes from multiple MSigDB gene sets, these being: BIOCARTA_COMP_PATHWAY, HALLMARK_COMPLEMENT, KEGG_COMPLEMENT_AND_COAGULATION_CASCADES, REACTOME_COMPLEMENT_CASCADE, BIOCARTA_ALTERNATIVE_PATHWAY, BIOCARTA_CLASSIC_PATHWAY. Graphical representation was done using ggplot2 (v3.3.2) or ComplexHeatmap (REF), or GraphPadPrism.

Statistical analysis: For each sample analyzed by RT-DC, the median measurement of over 500 cells was graphed as an individual point. The mean \pm SEM of all median measurements for each neutrophil subset is depicted and analyzed with statistical tests, Graphs were generated in GraphPad Prism and statistical tests were performed as described in each figure.

Matched donors for proteomics

| SLE Donors | | Healthy Donors | |
|------------|-----|----------------|-----|
| Age | Sex | Age | Sex |
| 61 | F | 64 | F |
| 36 | F | 35 | F |
| 32 | F | 31 | F |
| 53 | F | 50 | F |
| 46 | F | 45 | F |
| Avg=45.6 | | Avg=45.0 | |

SLE Demographics and SLEDAI

| LE Num | Visit Date | Gender | Age | Year of Diagnosis | Disease duration years | Ethnicity | SLEDAI TOTAL AT FIRST APPOINTMENT | SLEDAI SEIZURE | SLEDAI PSYCHOSIS | SLEDAI OBS | SLEDAI VISUAL DISTURB | SLEDAI CRANIAL NERVE | SLEDAI LUPUS HEADACHE | SLEDAI CVA | SLEDAI VASCULITIS | SLEDAI ARTHRITIS | SLEDAI MYOSITIS | SLEDAI URINARY CAST | SLEDAI HEMATURIA | SLEDAI PROTEINURIA | SLEDAI PYURIA | SLEDAI RASH | SLEDAI ALOPECIA | SLEDAI MUCOSAL ULCERS | SLEDAI PLEURISY | SLEDAI PERICARDITIS | SLEDAI LOW COMPLEMENT | SLEDAI LNC DNA BIND | SLEDAI FEVER | SLEDAI THROMBOCYTOPENIA | SLEDAI LEUKOPENIA | SLEDAI TOTAL |
|-----------|------------|--------|-----|-------------------|------------------------|------------------|-----------------------------------|----------------|------------------|------------|-----------------------|----------------------|-----------------------|------------|-------------------|------------------|-----------------|---------------------|------------------|--------------------|---------------|-------------|-----------------|-----------------------|-----------------|---------------------|-----------------------|---------------------|--------------|-------------------------|-------------------|--------------|
| LE-19-375 | 10/18/2019 | F | 61 | 2000 | 20 | African American | 2 | 0 | 0 | 0 | 0 | 0 | 0 | 0 | 0 | 0 | 0 | 0 | 0 | 0 | 0 | 0 | 0 | 0 | 0 | 0 | 0 | 2 | 0 | 0 | 0 | 2 |
| LE-19-388 | 10/24/2019 | F | 36 | 2010 | 10 | Hispanic | 12 | 0 | 0 | 0 | 0 | 0 | 0 | 0 | 0 | 4 | 0 | 0 | 0 | 0 | 2 | 2 | 0 | 0 | 2 | 0 | 0 | 0 | 0 | 0 | 0 | 8 |
| LE-19-419 | 11/18/2019 | F | 34 | 2012 | 8 | Hispanic | 4 | 0 | 0 | 0 | 0 | 0 | 0 | 0 | 0 | 0 | 0 | 0 | 0 | 0 | 0 | 2 | 0 | 0 | 0 | 0 | 0 | 2 | 0 | 0 | 0 | 4 |
| LE-19-433 | 11/25/2019 | F | 53 | 1992 | 28 | Caucasian | 0 | 0 | 0 | 0 | 0 | 0 | 0 | 0 | 0 | 0 | 0 | 0 | 0 | 0 | 0 | 0 | 0 | 0 | 0 | 0 | 0 | 0 | 0 | 0 | 0 | 0 |
| LE-19-432 | 11/25/2019 | F | 46 | 2003 | 17 | Hispanic | 8 | 0 | 0 | 0 | 0 | 0 | 0 | 0 | 4 | 0 | 0 | 0 | 0 | 0 | 0 | 0 | 0 | 0 | 0 | 2 | 2 | 0 | 0 | 0 | 0 | 8 |

Lab

| LE Num | Visit Date | Weight Kg | Height Cm | BMI | C3 | C4 | Anti-dsDNA | AMA | ENA | Anti-Sjogren's sy. A | Anti-Sjogren's sy. B | Anti-Smith(SM) | Anti-SmRNP | Date ENA |
|-----------|------------|-----------|-----------|------|-------|------|------------|--------------------|------|----------------------|----------------------|----------------|------------|------------|
| LE-19-375 | 10/18/2019 | 97.3 | 167.4 | 34.7 | 128 | 12.9 | 171 | 11.1 (11/25/2015) | neg | <0.2 | <0.2 | 0.2 | 0.3 | 11/25/2015 |
| LE-19-388 | 10/24/2019 | 125.2 | 155.8 | 51.6 | 84.6 | 9.7 | neg | 10.2 (7/9/2013) | >200 | <0.2 | 0.3 | >8.0 | 6.8 | 4/7/2017 |
| LE-19-419 | 11/18/2019 | 92 | 160.1 | 35.9 | 91 | 14.2 | >1000 | >12.0 (12/20/2012) | neg | neg | neg | neg | neg | 9/25/2017 |
| LE-19-433 | 11/25/2019 | 89.8 | 155.2 | 37.3 | 125.8 | 22.3 | neg | 1.3 (6/25/2015) | neg | neg | neg | neg | neg | 6/25/2015 |
| LE-19-432 | 11/25/2019 | 98.3 | 159.8 | 38.5 | 98.4 | 8.3 | 59 | >12.0 (6/8/2015) | >200 | 3.2 | <0.2 | >8.0 | 7.1 | 9/25/2017 |

Medications

| LE Num | Visit Date | HCQ [mg/day] | Prednisone [mg/day] | AZA [mg/day] | MTX [mg/week] | MMF [mg/day] | other | other | other | other | other | other |
|-----------|------------|--------------|---------------------|--------------|---------------|--------------|--------------------------------------|--|---------------------|---------------------------|------------------------|-----------------------------|
| LE-19-375 | 10/18/2019 | 400 | 5 | 100 | No | No | Losartan/HCTZ 50/12.5 mg PO daily | Metformin 1 gram BID | Prilosec 20mg daily | Synthroid 75 mcg daily | | |
| LE-19-388 | 10/24/2019 | 400 | 60 | No | No | No | Albuterol 90 mcg/actuation as needed | Pantoprazole 40 mg daily | Xarelto 20 mg daily | Atorvastatin 40 mg daily, | Toprol XL 25 mg daily, | Levothyroxine 150 mcg daily |
| LE-19-419 | 11/18/2019 | 400 | 10 | No | No | 2000 | Eliquis 5mg twice a day | Medroxyprogesterone 104 milligrams subcutaneous, | | | | |
| LE-19-433 | 11/25/2019 | No | 5 | No | 10 | No | Simvastatin 20mg daily | Synthroid 125mcg daily | | | | |
| LE-19-432 | 11/25/2019 | 400 | 6 | No | 25 | No | Tofacitinib 5mg BID | Acyclovir 400mg daily for prophylaxis | | | | |

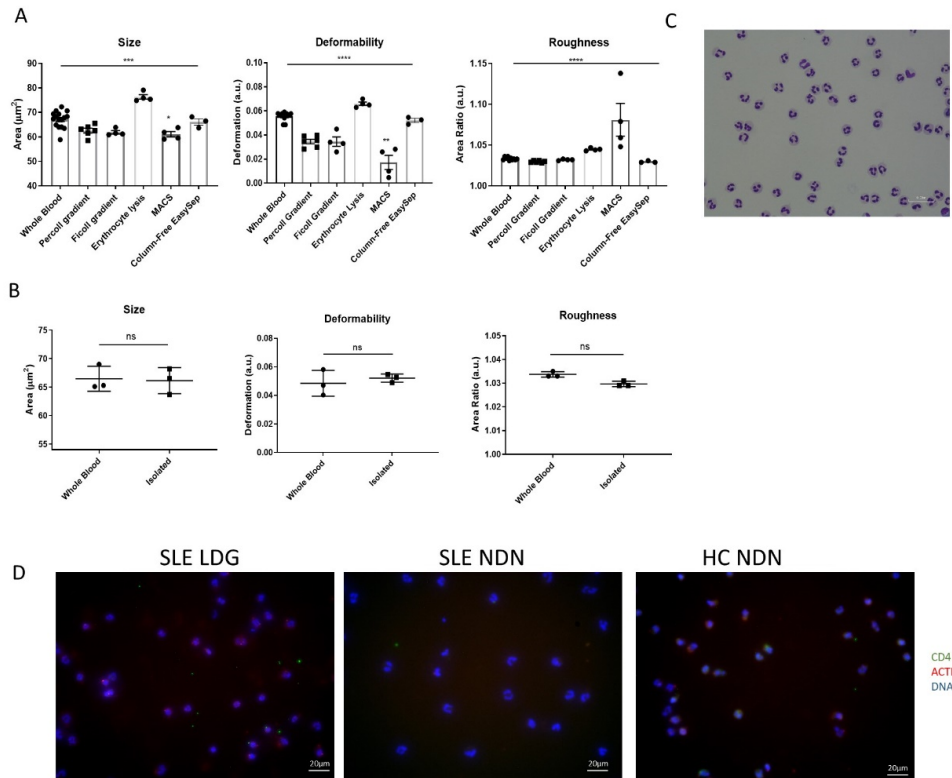
Supplementary Table 1. Demographic and clinical characteristics of SLE patients (n=5) and HC volunteers (n=5) donating blood for proteomics and phosphoproteomic analysis of LDGs and NDNs.

| Sex | Age | Race | SLEDAI on Day of Visit |
|-----|-----|------------------|------------------------|
| F | 36 | Caucasian | 4 |
| F | 42 | Caucasian | 2 |
| F | 22 | Caucasian | 0 |
| F | 24 | Caucasian | 2 |
| F | 58 | Caucasian | 0 |
| F | 23 | Caucasian | 2 |
| F | 49 | Asian | 0 |
| F | 56 | Caucasian | 2 |
| F | 31 | Caucasian | 2 |
| F | 59 | Hispanic | 2 |
| F | 60 | African American | 0 |
| F | 34 | Hispanic | 0 |
| F | 46 | Asian | 0 |
| F | 56 | Asian | 0 |
| F | 31 | Hispanic | 4 |
| F | 40 | Hispanic | 0 |
| F | 64 | Asian | 0 |
| F | 71 | Caucasian | 0 |
| F | 37 | African American | 0 |
| F | 61 | African American | 2 |
| F | 30 | Hispanic | 2 |
| F | 36 | Hispanic | 12 |
| F | 6 | Asian | 14 |
| F | 34 | Hispanic | 8 |
| F | 70 | African American | 0 |
| F | 47 | Asian | 4 |
| F | 55 | Asian | 4 |
| F | 82 | Caucasian | 2 |
| F | 34 | Asian | 8 |
| F | 25 | Hispanic | 0 |
| F | 53 | Caucasian | 0 |
| F | 35 | Hispanic | 2 |
| F | 49 | Hispanic | 2 |
| F | 57 | Caucasian | 4 |
| F | 58 | Hispanic | 0 |
| F | 39 | Hispanic | 4 |
| F | 54 | Hispanic | 4 |
| F | 35 | Hispanic | 12 |
| F | 64 | Asian | 2 |
| F | 31 | Hispanic | 4 |
| F | 50 | Hispanic | 0 |
| F | 56 | Asian | 2 |
| F | 29 | Hispanic | 0 |
| F | 25 | Hispanic | 0 |

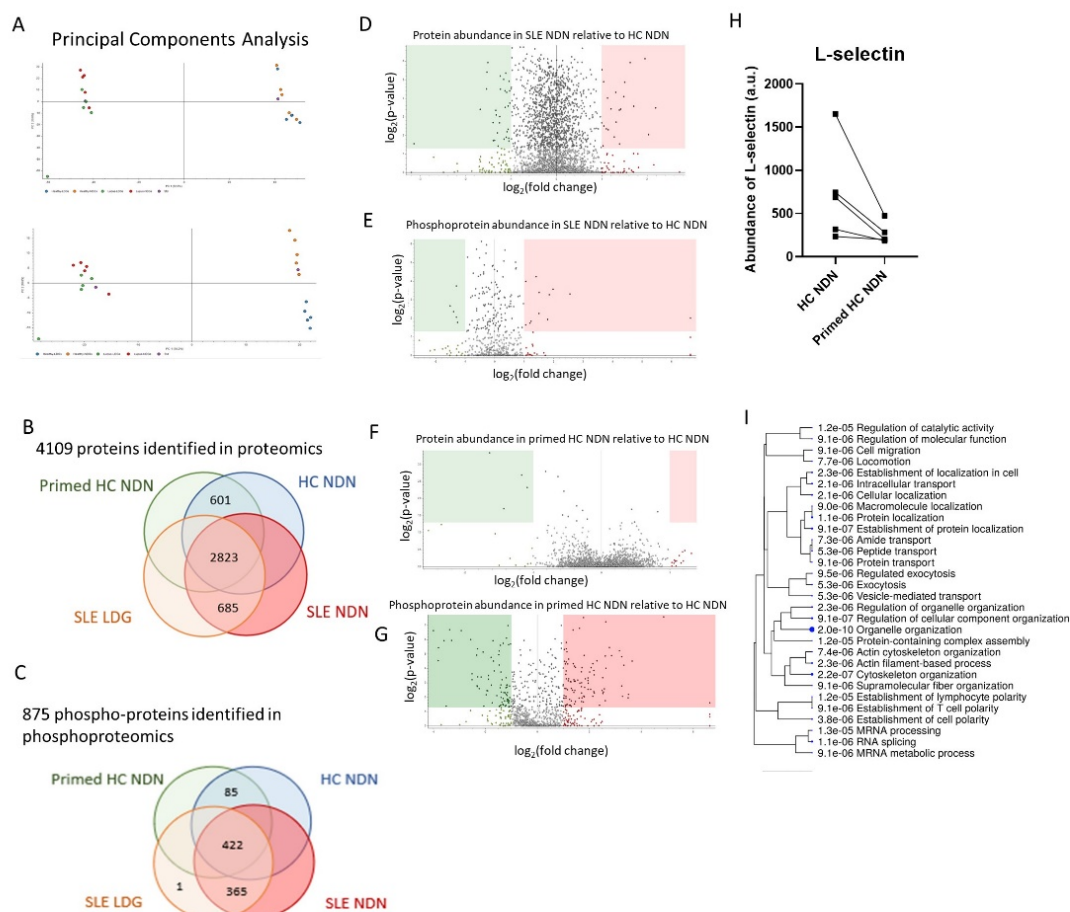
Supplementary Table 2. Demographic and clinical characteristics of all SLE patients donating blood for this study. SLEDAI for the first top nine patients on the table is based on clinical and serological activity, while SLEDAI for the rest of the patients also includes data from CBC and urinalysis.

| Gene Name | Protein Accession | Protein Description | Phosphopeptide Sequence |
|-----------|-------------------|--|-------------------------|
| PECAM1 | P16284 | Platelet endothelial cell adhesion molecule | YsRTEGSLDGT |
| ADAM22 | Q9P0K1 | Disintegrin and metalloproteinase domain-containing protein 22 | LSVVHTNYAK |
| DOCK5 | Q9H7D0 | Dedicator of cytokinesis protein 5 | APEPDLMSPTR |
| PIEZO1 | Q92508 | Piezo-type mechanosensitive ion channel component 1 | SGsEEAVTDPGER |
| LCP1 | P13796 | Plastin-2 | GsVSDEEMMELR |
| LCP1 | P13796 | Plastin-2 | GsVSDEEMMELR |
| LCP1 | P13796 | Plastin-2 | EGEsLEDLMK |
| PAK1 | Q13153 | Serine/threonine-protein kinase PAK 1 | YMsFTDK |
| PXN | P49023 | Paxillin | TSSVSNPQDSVGSPCSR |
| ZYX | Q15942 | Zyxin | GPPAsSPAPAK |
| ZYX | Q15942 | Zyxin | sPGAPGPLTLK |
| ARHGEF2 | Q92974 | Rho guanine nucleotide exchange factor 2 | QELGsPEER |
| ARHGEF2 | Q92974 | Rho guanine nucleotide exchange factor 2 | SEsLESPr |
| ARHGAP25 | P42331 | Rho GTPase-activating protein 25 | DIPLsPPAQK |
| ARHGAP25 | P42331 | Rho GTPase-activating protein 25 | GDTLAsPNSETGPGK |
| IQGAP2 | Q13576 | Ras GTPase-activating-like protein IQGAP2 | YGsIVDDER |
| WASF2 | Q9Y6W5 | Wiskott-Aldrich syndrome protein family member 2 | SsTIQDQK |
| CORO1A | P31146 | Coronin-1A | AAPEASGtPSSDAVSR |

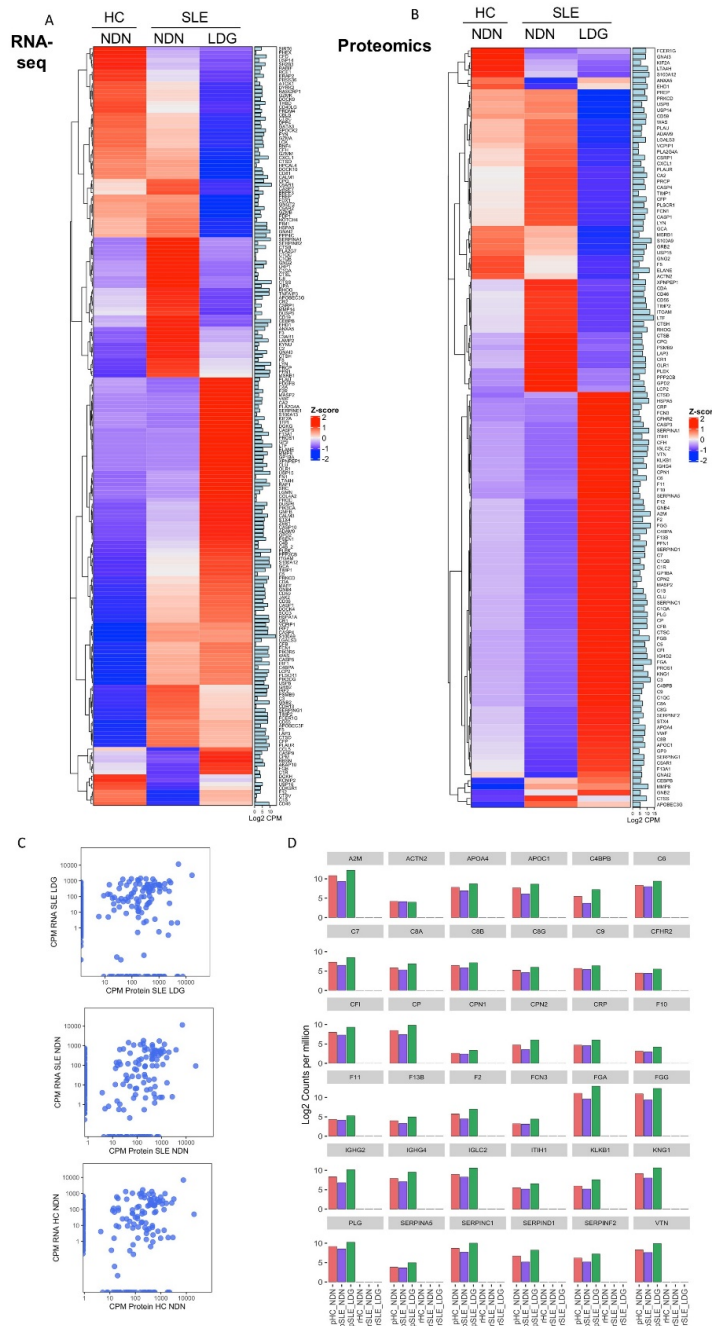
Supplementary Table 3. Phospho-site information for phosphoproteins referenced in the manuscript. Information for all phosphoproteins identified can be found in the PRIDE database. Lowercase letter indicates site of phosphorylation.



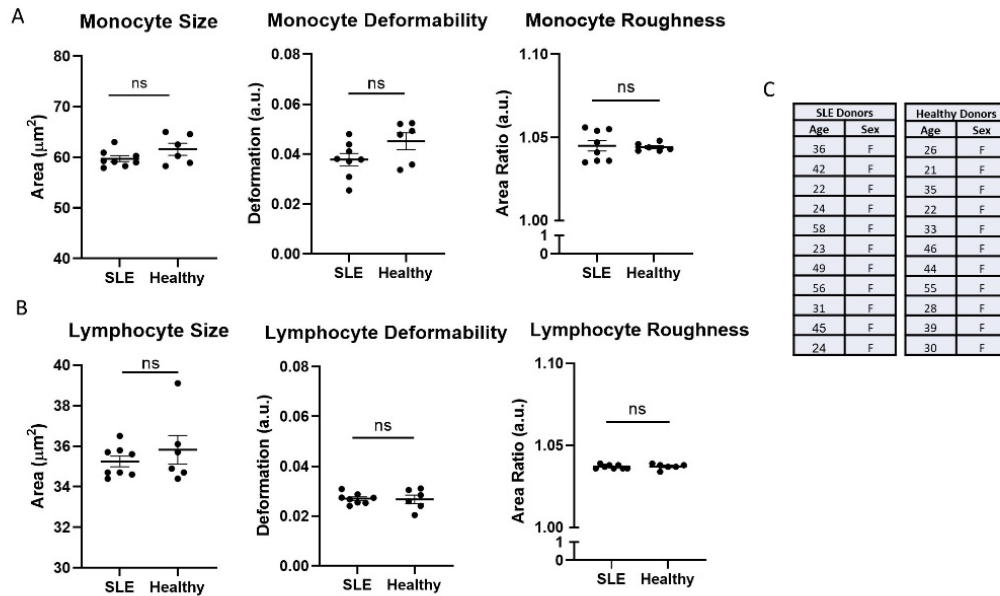
Supplementary Figure 1. Isolation of neutrophils was controlled to conserve mechanical properties observed in whole blood. (A) Biomechanical profiling by RT-DC of neutrophils in whole blood and following various isolation techniques (n≥3). Significance was established by Kruskal-Wallis test with a post hoc Dunn's test to compare isolated neutrophils to neutrophils in whole blood. (B) Isolation of neutrophils by density gradient, followed by a StemCell EasySep Column-free negative isolation strategy yields neutrophils biomechanically identical to their whole blood counterparts by RT-DC and (C) >98% pure by cytopsin (n=3). Significance was established by Mann-Whitney U-test. For each sample analyzed by RT-DC, the median of >500 neutrophils was graphed and the mean±SEM for each cell subset was depicted. Significance was set at *p<0.05, **p<0.01, ***p<0.001, ****p<0.0001, ns=not significant. (D) Neutrophil preparations did not show significant platelet contamination, as assessed by staining with platelet markers (images representatively of n=6).



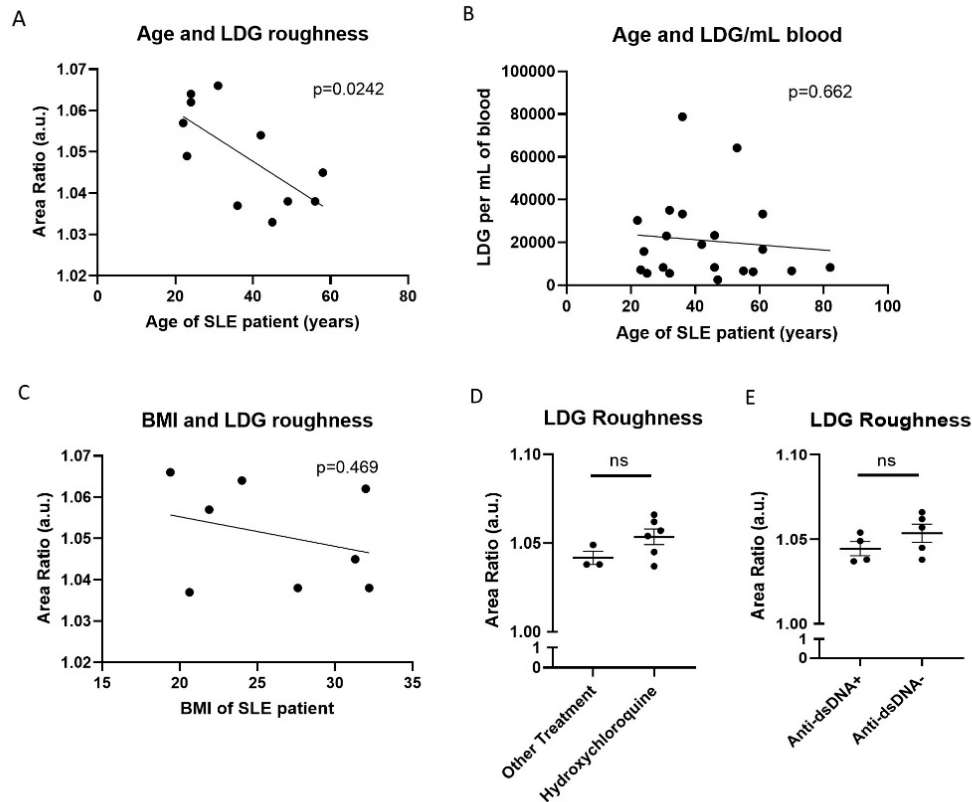
Supplementary Figure 2. Proteomics analysis of SLE LDGs, SLE NDNs, HC NDNs, and primed HC NDNs. (A) Principal components analysis of proteomics and phospho-proteomics data (n=5 healthy volunteers, n=5 SLE patients). (B) Distribution of 4109 identified proteins across all neutrophil subsets. (C) Distribution of 875 identified phospho-proteins across all neutrophil subsets. Volcano plots show separation between SLE NDN and HC NDN proteomes (D) and phosphoproteomes (E). The upregulated (red) and downregulated (green) (phospho)proteomes are SLE NDNs, as HC NDNs are the reference (phospho)proteome. Volcano plots show separation between primed HC NDN and unstimulated HC NDN proteomes (F) and phosphoproteomes (G). The upregulated (red) and downregulated (green) (phospho)proteomes are primed HC NDNs as unstimulated HC NDNs are the reference (phospho)proteome. (H) Abundance of L-selectin in arbitrary units. Results are mean \pm SEM. (I) Gene ontology biological process analysis highlighting biological networks associated with proteins differentially phosphorylated in SLE NDNs relative to HC NDNs. Proteins with differential phosphorylation at a specific phosphosite in at least 4/5 samples and with an abundance ratio less than 0.5 or greater than 1.5 were included and significance was established by false discovery rate (FDR).



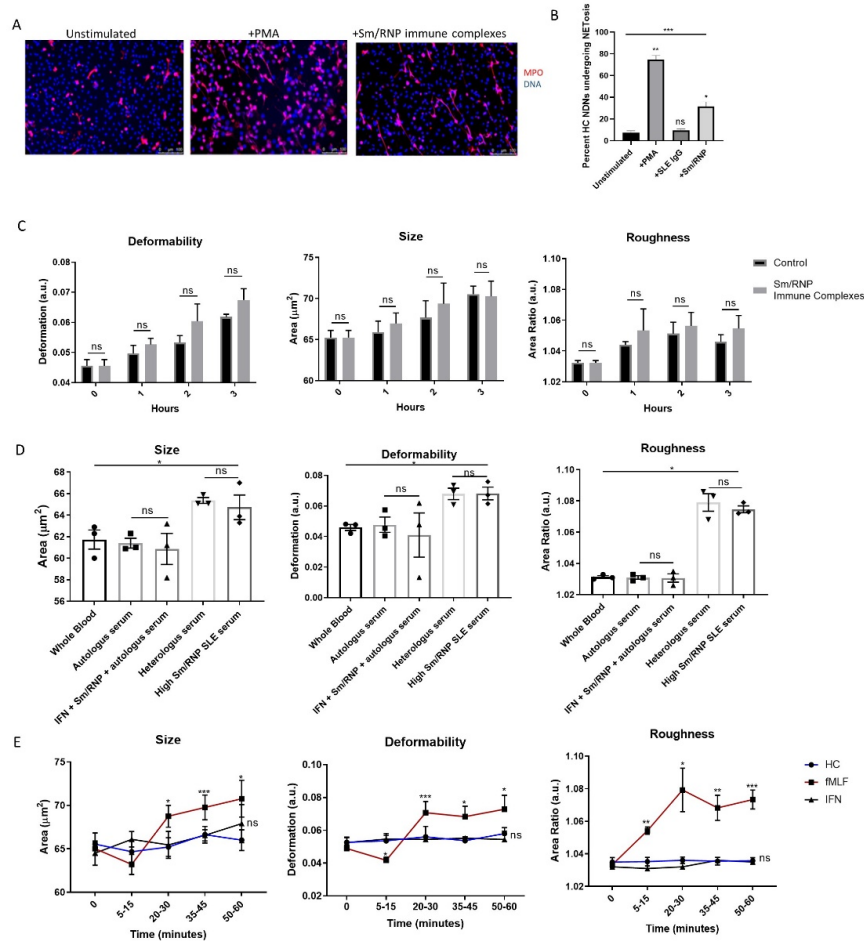
Supplementary Figure 3. Investigation of proteins identified by mass spectrometry at the transcript level. Relative expression of mRNA transcripts (A) and proteins (B) in HC NDNs, SLE NDNs, and SLE LDGs. C) Comparison of mRNA transcript expression and protein expression in SLE LDGs, SLE NDNs, and HC NDNs. D) Genes not detected by transcriptomics in HC NDNs, SLE NDNs, or SLE LDGs, but which encode proteins detected by mass spectrometry.



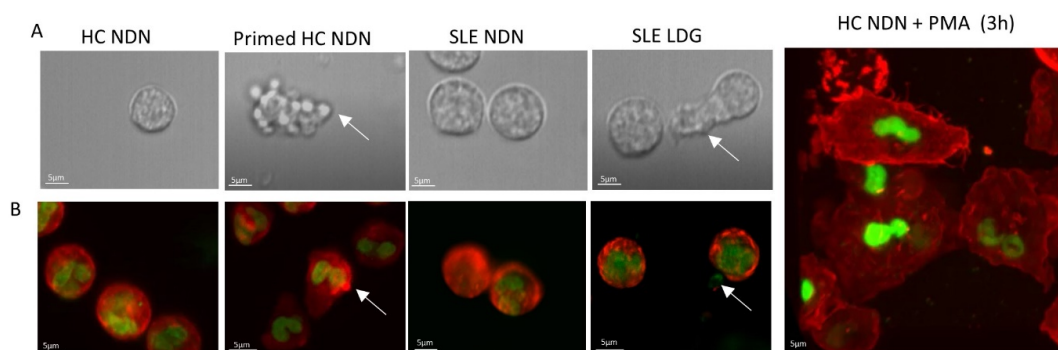
Supplementary Figure 4. The biomechanical properties of lymphocytes and monocytes do not differ between healthy individuals and clinically quiescent SLE. (A) Biomechanical profiling of monocytes from SLE patients (n=8) and healthy volunteers (n=6) by RT-DC. (B) Biomechanical profiling of lymphocytes from SLE patients (n=8) and healthy volunteers (n=6) by RT-DC. For each sample analyzed by RT-DC, the median measurement of over 300 lymphocytes or monocytes is graphed and the mean \pm SEM for each cell subset is depicted. Significance was established by Mann-Whitney U-tests and was set at $*p < 0.05$, ns=not significant. (C) Sex and age-matched demographics of HC donors (n=11) and SLE patients (n=11) giving samples analyzed by RT-DC for neutrophil biomechanical properties.



Supplementary Figure 5. Association of biomechanical properties with SLE clinical features. (A) Correlation of LDG roughness with SLE patient age in SLE (n=11). (B) Correlation of LDG numbers with age of SLE patient (n=21). (C) Correlation of LDG roughness with BMI in SLE patients (n=8). For all correlations, significance was assessed by linear regression analysis and set at $*p \leq 0.05$, ns=not significant. (D) LDG roughness in SLE subjects treated with hydroxychloroquine (n=5) or other treatments (n=3). (E) LDG roughness in SLE patients positive (n=4) or negative (n=4) for serum anti-dsDNA antibodies. Roughness was determined by RT-DC. The median roughness measurement from over 100 neutrophils from each subject is graphed and the mean \pm SEM for each treatment or clinical category is depicted. For D and E, significance was established by Mann-U-Whitney tests and set at $*p < 0.05$, ns=not significant.

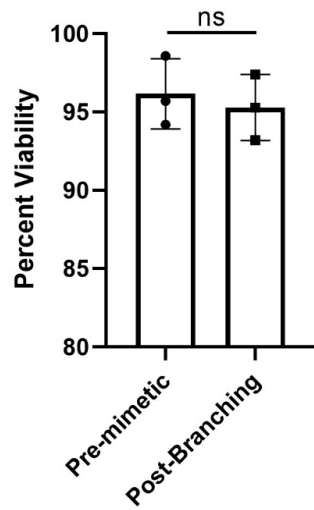


Supplementary Figure 6. SLE-relevant immune stimuli do not significantly modulate biomechanical properties of healthy control neutrophils. (A, B) Sm/RNP immune complexes used for RT-DC assay are shown to be functional by inducing in vitro NET formation in HC NDNs (n=6). Red indicates MPO, blue indicates DNA. (C) Biomechanical profiling of HC NDNs incubated with 10ng/ μ l Sm/RNP immune complexes or with DMSO over three hours by RT-DC (n=3). (D) Biomechanical profiling of HC NDNs treated with autologous HC, heterologous HC, or heterologous, active SLE patient serum for 45 minutes by RT-DC. Some NDNs were also treated with 10ng/ μ l Sm/RNP immune complexes and 1000units/mL IFN α (n=3). (E) Biomechanical profiling over time of neutrophils in HC blood stimulated with DMSO, 100nM fMLF, or 1000units/mL IFN α (n=3). For each sample analyzed by RT-DC, the median of >500 neutrophils was graphed and the mean \pm SEM for each cell subset was depicted. For C & E, unstimulated neutrophils treated with DMSO were compared to stimulated neutrophils from autologous donors at matched time points. For D, neutrophils from autologous donors treated with different serum samples were compared. Significance was established by Kruskal-Wallis test (B, C, E) or Friedman's test (D) with post hoc Dunn's tests for multiple comparisons and set at *p<0.05, **p<0.01, ***p<0.001, ns=not significant.

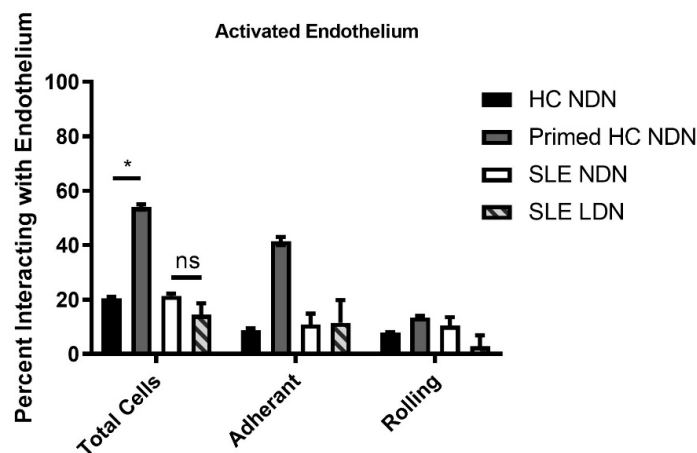


Supplementary Figure 7. Brightfield microscopy and fluorescence lattice light-sheet microscopy capture differences in neutrophil biophysical properties with high resolution.

(A) Unstained neutrophils imaged by brightfield microscopy (n=3 SLE patients, n=3 HC volunteers). (B) Neutrophils stained for actin (red) and DNA (green) by SiR-actin probe and sytox green, respectively, and imaged by lattice light-sheet fluorescence microscopy (n=2 SLE patients, n=2 HC volunteers). Some HC NDNs were stimulated with 25nM PMA to induce NETs. White arrows indicate rounded protrusions in 100% of primed HC NDNs, visible in unstained and stained neutrophils. White arrows indicate irregular protrusions observed in ~30% of unstained SLE LDGs. Irregular protrusions were visible in a single stained SLE LDG depicted, but the majority of stained SLE LDGs appeared round. Stained SLE LDGs did not resemble HC NDNs undergoing PMA-stimulated NET formation. See supplementary video files 1-4 for more detail.

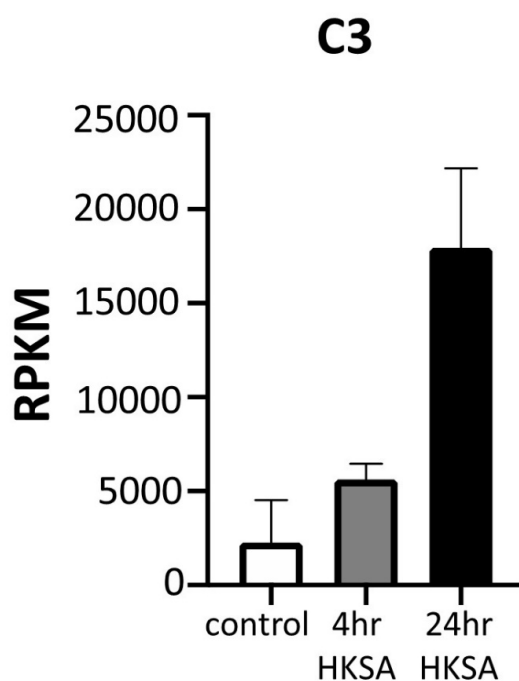


Supplementary Figure 8. The MMM does not impact neutrophil viability. (A) Neutrophil viability before and after transiting the microvasculature mimetic (n=3). Significance was established by paired Student's T-test and set at *p<0.05, ns=not significant.



Supplementary Figure 9. SLE LDGs do not display enhanced adherence to activated endothelial cells in a two-dimensional system of flow.

The percentage of neutrophils interacting with activated endothelium under a system of flow (n=3 HC volunteers, n=3 SLE patients). Results are mean \pm SEM with comparisons between autologous SLE LDGs and SLE NDNs as well as autologous primed HC NDNs and HC NDNs. Significance was established by Kruskal-Wallis test with post hoc Dunn's tests for multiple comparisons and set at **p \leq 0.01, ns=not significant.



Supplementary Figure 10. C3 expression is upregulated at the transcript level in neutrophils activated by *Staphylococcus aureus*. mRNA expression of C3 in HC NDNs cultured with heat-killed *Staphylococcus aureus* for indicated time points. mRNA expression determined by RNA-SEQ using two HC donors. Data in GEO GSE73313.

Supplementary video files:

Video File 1: Unstimulated HC NDNs imaged by brightfield lattice light-sheet microscopy.

Video File 2: Primed HC NDNs imaged by brightfield lattice light-sheet microscopy.

Video File 3: SLE NDNs imaged by brightfield lattice light-sheet microscopy.

Video File 4: SLE LDGs imaged by brightfield lattice light-sheet microscopy.

Supplementary References

1. Aringer M, Costenbader K, Daikh D, et al. 2019 European League Against Rheumatism/American College of Rheumatology Classification Criteria for Systemic Lupus Erythematosus. *Arthritis & Rheumatology* 2019;71(9):1400-12. doi: 10.1002/art.40930
2. Hochberg MC. Updating the American college of rheumatology revised criteria for the classification of systemic lupus erythematosus. *Arthritis & Rheumatism* 1997;40(9):1725-25. doi: 10.1002/art.1780400928
3. Haslett C, Guthrie LA, Kopaniak MM, et al. Modulation of multiple neutrophil functions by preparative methods or trace concentrations of bacterial lipopolysaccharide. *The American Journal of Pathology* 1985;119(1):101-10.
4. Clark RA, Nauseef WM. Isolation and Functional Analysis of Neutrophils. *Curr Protoc Immunol* 1996;19(1):7.23.1-7.23.17. doi: 10.1002/0471142735.im0723s19
5. Lood C, Blanco LP, Purmalek MM, et al. Neutrophil extracellular traps enriched in oxidized mitochondrial DNA are interferogenic and contribute to lupus-like disease. *Nature medicine* 2016;22(2):146-53. doi: 10.1038/nm.4027
6. Yang F, Shen Y, Camp DG, 2nd, et al. High-pH reversed-phase chromatography with fraction concatenation for 2D proteomic analysis. *Expert Rev Proteomics* 2012;9(2):129-34. doi: 10.1586/epr.12.15
7. Ting L, Rad R, Gygi SP, et al. MS3 eliminates ratio distortion in isobaric multiplexed quantitative proteomics. *Nature Methods* 2011;8(11):937-40. doi: 10.1038/nmeth.1714
8. Wühr M, Haas W, McAlister GC, et al. Accurate multiplexed proteomics at the MS2 level using the complement reporter ion cluster. *Anal Chem* 2012;84(21):9214-21. doi: 10.1021/ac301962s [published Online First: 2012/10/25]
9. Käll L, Canterbury JD, Weston J, et al. Semi-supervised learning for peptide identification from shotgun proteomics datasets. *Nature Methods* 2007;4(11):923-25. doi: 10.1038/nmeth1113
10. Kall L, Storey JD, MacCoss MJ, et al. Posterior error probabilities and false discovery rates: two sides of the same coin. *J Proteome Res* 2008;7(1):40-4. doi: 10.1021/pr700739d [published Online First: 2007/12/07]
11. Brosch M, Yu L, Hubbard T, et al. Accurate and sensitive peptide identification with Mascot Percolator. *J Proteome Res* 2009;8(6):3176-81. doi: 10.1021/pr800982s [published Online First: 2009/04/03]
12. Spivak M, Weston J, Bottou L, et al. Improvements to the percolator algorithm for Peptide identification from shotgun proteomics data sets. *J Proteome Res* 2009;8(7):3737-45. doi: 10.1021/pr801109k [published Online First: 2009/04/24]
13. McAlister GC, Huttlin EL, Haas W, et al. Increasing the multiplexing capacity of TMTs using reporter ion isotopologues with isobaric masses. *Anal Chem* 2012;84(17):7469-78. doi: 10.1021/ac301572t [published Online First: 2012/08/14]
14. Cominetti O, Nunez Galindo A, Corthesy J, et al. Proteomic Biomarker Discovery in 1000 Human Plasma Samples with Mass Spectrometry. *J Proteome Res* 2016;15(2):389-99. doi: 10.1021/acs.jproteome.5b00901 [published Online First: 2015/12/02]
15. Wood AJT, Vassallo AM, Ruchaud-Sparagano M-H, et al. Complement C5a impairs phagosomal maturation in the neutrophil through phosphoproteomic remodelling. *bioRxiv* 2020:2020.01.17.907618. doi: 10.1101/2020.01.17.907618

16. Ge SX, Jung D, Yao R. ShinyGO: a graphical gene-set enrichment tool for animals and plants. *Bioinformatics* 2019 doi: 10.1093/bioinformatics/btz931
17. Zhou Y, Zhou B, Pache L, et al. Metascape provides a biologist-oriented resource for the analysis of systems-level datasets. *Nature Communications* 2019;10(1):1523. doi: 10.1038/s41467-019-09234-6
18. Otto O, Rosendahl P, Mietke A, et al. Real-time deformability cytometry: on-the-fly cell mechanical phenotyping. *Nature Methods* 2015;12:199. doi: 10.1038/nmeth.3281
<https://www.nature.com/articles/nmeth.3281#supplementary-information>
19. Herbig M, Kräter M, Plak K, et al. Real-Time Deformability Cytometry: Label-Free Functional Characterization of Cells. In: Hawley TS, Hawley RG, eds. *Flow Cytometry Protocols*. New York, NY: Springer New York 2018:347-69.
20. Herbig M, Mietke A, Müller P, et al. Statistics for real-time deformability cytometry: Clustering, dimensionality reduction, and significance testing. *Biomicrofluidics* 2018;12(4):042214. doi: 10.1063/1.5027197
21. Mietke A, Otto O, Girardo S, et al. Extracting Cell Stiffness from Real-Time Deformability Cytometry: Theory and Experiment. *Biophysical Journal* 2015;109(10):2023-36. doi: <http://dx.doi.org/10.1016/j.bpj.2015.09.006>
22. Toepfner N, Herold C, Otto O, et al. Detection Of Human Disease Conditions By Single-Cell Morpho-Rheological Phenotyping Of Whole Blood. *bioRxiv* 2017 doi: 10.1101/145078
23. Ekpenyong AE, Toepfner N, Fiddler C, et al. Mechanical deformation induces depolarization of neutrophils. *Science Advances* 2017;3(6) doi: 10.1126/sciadv.1602536